UNIVERSITY OF CALIFORNIA
Santa Barbara

Understanding Nanoemulsion Formation and Developing a Procedure for Porous Material Growth using Assembled Nanoemulsions

A Thesis submitted in partial satisfaction of the

requirements for the degree Master of Science

in Chemical Engineering

by

Vahagn Frounzig Yeranossian

Committee in charge:

Professor Matt Helgeson, Chair

Professor Brad Chmelka

Professor Todd Squires

March 2015

The thesis of Vahagn Frounzig Yeranossian is approved.

_____

Todd Squires

_____

Brad Chmelka

_____

Matt Helgeson, Committee Chair

May 2015

ACKNOWLEDGEMENTS

I would like to thank my family who were very supportive of me during my work. I would like to thank my advisors Professors Matt Helgeson and Brad Chmelka for their advice through the years in my experimental work and my thesis. Finally, I would like to thank my friends for their support through my trials and through helping me find a new career path.

ABSTRACT

Understanding Nanoemulsion Formation and Developing a Procedure for Porous Material Growth using Assembled Nanoemulsions

by

Vahagn Frounzig Yeranossian

Nanoemulsions as an emerging technology have found many applications in consumer products, drug delivery, and even particle formation. However, knowledge gaps exist in how some of these emulsions are formed, specifically what pathways are traversed to reach the final state. Moreover, how these pathways affect the final properties of the nanoemulsions would affect the applications that these droplets possess. Some nanoemulsions possess unique properties, including the assembly of droplets. While the assembly of droplets is being studied in the Helgeson lab, work must be done to understand how the assembly itself could be used to control the growth of porous materials, such a hydrogels. Thus, this thesis aims to address two factors of nanoemulsions: the formation of water-in-oil nanoemulsions and the use of assemblying droplets in oil-in-water nanoemulsions to form macroporous hydrogels.

To elucidate the formation mechanism of water-in-oil nanoemulsions, a combination of dynamic light scattering and small angle neutron scattering were used to study the intermediate and final states of the nanoemulsion during its formation. These nanoemulsions were prepared by slowly adding water to an oil and surfactant mixture and were diluted to effectively measure using scattering techniques without multiple scattering events. To develop a procedure to use assembled nanoemulsions for the growth of porous materials, a combination of optical microscopy and diffusional studies were employed. Optical microscopy images taken at various

stages of the procedure help elucidate how the pore sizes of the final porous material is related to the droplet-rich domains of the assembled nanoemulsion. Meanwhile, diffusional measurements help confirm the size and interconnectedness of the macropores.

From the work done in the completion of my thesis, the formation mechanism of the water-in-oil nanoemulsion studied has been elucidated. The neutron scattering measurements show that during the formation of the nanoemulsion, a combination of droplets and vesicles form. The presence of vesicles provides insight into how chemical additives in the water would affect the final droplet properties. This insight can be used to design water-in-oil nanoemulsions to be used for the controlled synthesis of solid nanoparticles. Additionally, this work demonstrates a potential procedure for developing macroporous hydrogels using nanoemulsions that are assembled into droplet-rich and droplet-poor domains. Through mild UV cross-linking conditions and mild solvent extraction techniques, the pore sizes could be equivalent to the droplet-rich domain sizes. The final hydrogels can control diffusivity of molecules, giving them potential applications in drug delivery.

TABLE OF CONTENTS

LIST OF FIGURES

I. Introduction

A. Nanoemulsions

Nanoemulsions, metastable liquid dispersions with droplets ranging from 10-200 nm, are an important technology in drug delivery [1-5], consumer products [6-9], and particle synthesis [10-16]. The applications of nanoemulsions depend heavily on their properties, such as droplet size, stability, surface charge, etc. Some of these properties, namely size and stability of droplets, depend on the mechanism of emulsification. Nanoemulsions can be formed through low energy emulsification techniques, such as the phase inversion temperature method [17-19] or spontaneous emulsification [20], or high energy emulsification techniques, such as high pressure homogenization [7, 21, 22] or ultrasonication [23].

A common misconception about nanoemulsions is conflating them with microemulsions. As opposed to nanoemulsions, microemulsions are a few nanometers in diameter and are essentially swollen micelles. Thus, they are thermodynamically stable surfactant structures with some solvent dissolved within the micelles. As a result, they can only be formed spontaneously and their properties depend heavily on the chemistry of either liquid used to form the emulsion. Due to their small size, chemical sensitivity, and the vast body of work done studying microemulsions, microemulsions are not of interest for the presented work.

B. Low energy vs High energy emulsification

Nanoemulsions formed using high-energy techniques are produced by breaking apart larger droplets using high mechanical power, and thus the droplet size is independent of the specific droplet chemistry. While this allows for loading of drugs or precursor materials for synthesis, high energy techniques are energy intensive and can be difficult to scale up due to the

higher energy cost. Low energy techniques typically require the chemical potential of the two phases to spontaneously form a nanoemulsion without adding extra energy. Thus, low energy techniques are thermodynamically-driven kinetic processes that result in a metastable, non-equilibrium nanoemulsion. However, they can still use kinetic pathways to form droplets thus allowing for droplet size to be independent of droplet chemistry in a similar way as high energy techniques, but these techniques are much cheaper to scale up than their high energy counterparts. Moreover, understanding the kinetic pathways that the system takes to reach the final nanoemulsion state is not well understood and is thus of interest to us [17]. Understanding the kinetic pathway of low energy nanoemulsification would give us the ability to control the nanoemulsion's properties. Thus, such an understanding would allow them to be efficiently produced and give the potential for future scale-up.

C. Nanoemulsion Stability

While nanoemulsions can be formed spontaneously, they represent immiscible liquids with a high surface area and thus are not thermodynamically stable. Initially, nanoemulsion droplets are small enough that they avoid sedimentation [24]. The droplets, however, can grow under mechanisms that combine contents of droplets. Such droplet instability occurs primarily by two mechanisms [25]. The first is Ostwald ripening, whereby there is a thermodynamic driving force for the net transfer of the dispersed phase between small droplets through the continuous phase (due to sparing solubility) and the larger droplets. Ostwald ripening typically dominates when the droplets are less than 100 nm in diameter. The second is coalescence, whereby two droplets collide and fuse, adding their volumes together. Coalescence typically dominates when the droplets are greater than 100 nm in diameter. Below this size, coalescence is suppressed due

to the higher Laplace pressure inside the droplet. Both these mechanisms can cause droplets to grow large enough to sediment or cream, resulting in colloidal instability.

D. Oil-in-water vs Water-in-oil Nanoemulsions

Much work has been done developing several nanoemulsion systems. Specifically, significant work has been done in developing oil-in-water NE systems (O/W NE). These emulsions consist of nanoscopic oil droplets surrounded by water and colloidally stabilized by a surfactant. O/W NEs either use a charged surfactant to become colloidally stable due to long range electrostatic repulsions between the charged colloids or use a nonionic surfactant that use steric-hydration forces to deter coalescence [26]. Professor Helgeson has done extensive work developing a O/W NE system that can be used for consumer product applications and for producing particles for drug delivery applications [21, 27].

Compared to O/W NEs, water-in-oil nanoemulsions (W/O NE) are underdeveloped with only a handful of papers studying them. Some work has been done varying surfactant, water, and oil concentrations and compositions to determine optimal conditions for W/O NE formation [17, 28-32]. Most of these works utilize co-surfactant systems, where two surfactants help reduce interfacial tensions and reduce droplet sizes [3]. W/O NE droplets repel each other due to the reduction of configurational entropy of the surfactant chains from adjacent droplets when they overlap [33]. This steric barrier to coalescence allows W/O NEs to remain colloidally stable depending on the bulkiness of the surfactant tail.

E. Nanoemulsions for Controlling Material Synthesis

W/O NEs have the ability to confine aqueous compounds or reactions in droplets. Work has been done studying how W/O NEs can be used as vessels for the transdermal delivery of hydrophilic compounds [34-36] and as a platform for growing nanoparticles [10, 16]. Porras, *et al*. showed that the droplet sizes seemed well-correlated with the sizes of oxide nanoparticle grown within them, indicating confinement of the reaction in the droplet [16]. Similarly, O/W NEs can be used to confine the synthesis of hydrophobic reactions, such as polymerization or cross-linking of hydrophobic polymers to make polymer nanoparticles. The effect of particle confinement is theoretically the same regardless of the droplet chemistry.

Using the techniques of particle confinement within or outside of droplets, porous materials could also be formed by the assembly of these droplets. By causing droplets to aggregate without coalescing with small (1-2 nm) distances between droplets, materials that are grown outside or inside of droplets could be grown continuously with a continuous porous structure. Thus nanoemulsions could be used to control either individual particle growth or the porous structure of a larger network.

F. Objectives

Given the important applications of nanoemulsions, their versatility in material development, and the limited literature on the subject, the objectives of this work are to 1) develop and seek to understand the formation of a water-in-oil nanoemulsion that forms from a low energy emulsification (spontaneous emulsification) and 2) to develop a process to create and control porosity in hydrogel networks using the assembly of nanoemulsion droplets.

In order to understand the formation of water-in-oil nanoemulsions, the droplet sizes must be monitored under various processing conditions to find the conditions that most

effectively affect the droplet size. Knowledge of these variables can provide important insight into the nature of the formation mechanism, specifically whether it is a thermodynamic or kinetic mechanism. The next goal is to understand the formation mechanism itself, which requires *in situ* techniques to identify the structure of the nanoemulsion at intermediate states.

In order to control porosity in hydrogel networks using nanoemulsions, the growth of droplet-rich domains under temperature and time must be understood. The ways that the droplet-rich domains change under the processing conditions to form the hydrogel and extract the solvents must also be understood so the sizes of the hydrogel pores can be correlated with the droplet-rich domains of the phase-separated nanoemulsion. Finally, the effect of the controlled porosity in the hydrogel on the diffusion of molecules (to simulate drug delivery particles) must be understood.

II. Understanding the Formation and Stability of W/O Nanoemulsion

A. Introduction

In order to produce droplets that can act as a medium to control material growth, it is vital to understand both the formation mechanism and the stability of these droplets. As mentioned in Chapter I section D, much work has been done to understand the formation of oil-in-water nanoemulsions, but significantly less work has been done understanding water-in-oil (W/O) nanoemulsions. W/O nanoemulsions are important for the goal of material growth due to the fact that a large number of solution phase material chemistries require a hydrophilic environment (e.g. silica), so that the droplet could act as a container for material growth.

Some W/O nanoemulsions have been studied primarily using low energy [10, 28, 30, 37] emulsification techniques. However, few *in situ* studies have been performed during emulsification of W/O nanoemulsions, and so the previous studies provide little insight regarding the mechanisms of low-energy emulsification of these emulsions. This knowledge gap can be attributed to the fluid nature of the droplet interface, which makes these *in situ* studies challenging. However, by utilizing non-destructive techniques, such as neutron scattering, it is possible to gain this important insight into the formation mechanism of nanoemulsions. Moreover, this insight can provide an understanding of how different material chemistries, such as sol-gel reactions, might affect the droplet formation and stability. Specifically, understanding the formation mechanism and properties of a nanoemulsion can predict the largest size that materials can be grown.

While work has been done on finding optimal conditions for making nanoemulsions, little work has been done exploring the nanoemulsification mechanisms for low energy approaches. *In situ* analysis of the nanoemulsion microstructure throughout the formation

process is quite sparse, but is necessary to fully comprehend the factors that determine the nanoemulsion's properties.

B. Objectives

Knowing the kinetic pathway involved in forming the final nanoemulsion and how additives would affect the intermediate phases can allow us to predict important properties of the final droplets including droplet size and stability. Therefore, this work aims to understand the pathway of nanoemulsion formation through *in situ* and *ex* situ analysis to explain the size and stability of the final droplets.

Since a significant long term goal of this work is to control nanoparticle sizes synthesized within W/O NE droplets, being able to control the droplet sizes is vital. We hypothesize that stable emulsions with nanoscopic droplets could be formed using a low energy emulsification technique, or spontaneous nanoemulsification.

C. Methods

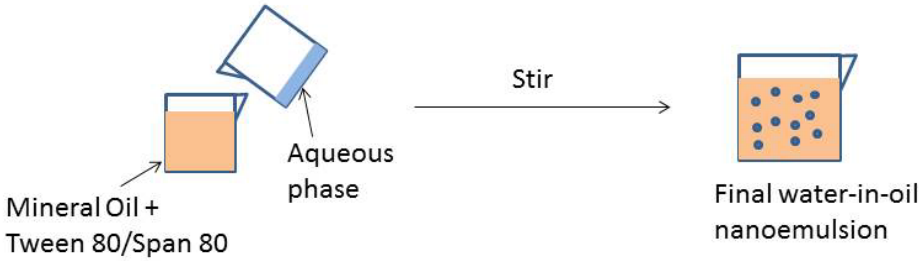

Figure 1. Procedure for forming water-in-oil nanoemulsions. The aqueous phase is slowly added to a mixture of oil and surfactants under continuous stirring. The final nanoemulsion is formed within an hour.

Figure 1 depicts the procedure for which the W/O NEs are produced: mineral oil is mixed with nonionic surfactants Span 80 and Tween 80 (all purchased from Sigma Aldrich) and, under constant stirring, DI water is added drop-wise. After 1 hour, the final nanoemulsion is formed. Nanoemulsions were formed using varied concentrations of surfactant and water and the droplet diameters were measured over time. To study the final properties of the

nanoemulsion, such as droplet diameter and stability, dynamic light scattering (DLS) is used. To prepare the nanoemulsions for DLS, they were diluted in mineral oil to approximately 0.5 vol% droplets. At this low droplet concentration DLS can provide accurate information about the droplet sizes and this information can be examined over time to understand the stability of the droplets.

We hypothesized that the nanoemulsions formed primarily through the swelling of surfactant micelles with water and the formation of other surfactant-water aggregates, such as vesicles. To test this hypothesis, we used small angle neutron scattering (SANS) at various intermediate concentrations of D_2O to simulate the progression of droplet formation during the emulsification process. To prepare samples for SANS, nanoemulsion samples were prepared using low water concentrations in an attempt to elucidate intermediate structures. SANS measurements were performed at the neutron scattering facility at the National Institute of Standards & Technology (NIST) Center for Neutron Research (NCNR). Measurements were taken on the NG-7 detector with a q-range of 0.0009 A^{-1} to 0.6 A^{-1} and the 10CB sample environment. All samples are contained in standard 1 mm titanium scattering cells with quartz windows. All samples were prepared with D_2O instead of water to maximize scattering contrast between the dispersed and continuous phases. Analysis of SANS data was done by fitting desired models to the data using the NCNR Igor Pro SANS package [38]. Parameters from the fitted models were used to estimate the properties of the nanoemulsion, namely particle sizes.

D. Results & Discussion

1. Size range and stability of nanoemulsion

To begin our studies, we explored the range of sizes that could be formed with our nanoemulsion formation procedure. We anticipated that we could acquire nanoscopic droplets by

varying total surfactant concentration because surfactant concentration affects the total contact area between the oil and water that can be stabilized. Specifically, we expected the droplet size to asymptotically decrease toward a constant droplet size distribution as the total surfactant concentration increased. This asymptote is expected to arise from the higher LaPlace pressure of small droplets countering the reduction of surface tension due to higher surfactant concentrations.

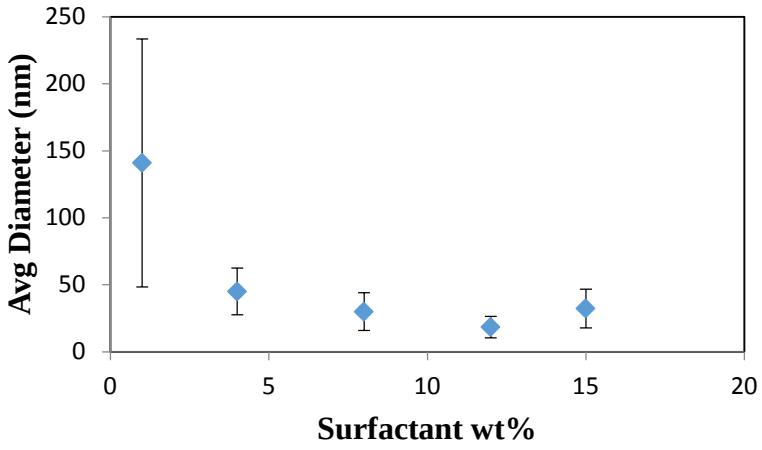

Figure 2a. 10 wt% water-in-mineral oil nanoemulsions formed at different surfactant concentrations with a fixed Span 80:Tween 80 ratio of 55:45 by volume.

Figure 2a presents a typical relation between average diameter and the total surfactant concentration, this data specifically represents emulsions with 10 wt% water. The error bars for this figure and the rest of the droplet size measurements represent the standard deviation of the average droplet size, based on the droplets polydispersity as measured by DLS. By varying the total concentration of surfactant (keeping the Span 80:Tween 80 ratio constant at 55:45 by volume), the emulsification method forms droplets with average diameters ranging from 20 nm to 150 nm. From the figure above, it appears as though a minimum in the final droplet diameter occurs at 12 wt% surfactant. Such a minimum is reproducible, and has only been demonstrated in a small number of O/W systems [39]. However, its existence is poorly explained. The origin

of this minimum droplet size at intermediate surfactant concentration will be discussed later, and may be due to the formation of multilamellar vesicles at high surfactant concentrations, which could inhibit the formation of smaller droplets.

We also examined how varying the amount of water in the nanoemulsion affects the final droplet size distribution. We anticipated that more water should result in larger droplets, assuming surfactant concentration is held constant. The constant surfactant concentration should fix the interfacial area that can be stabilized, so increasing the volume of the dispersed phase should increase the average droplet size.

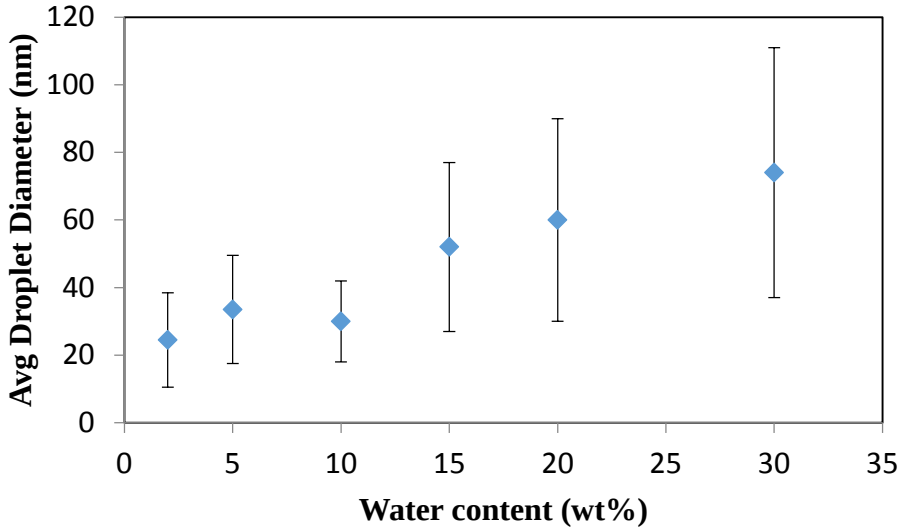

Figure 2b. Varying the amount of water in nanoemulsions with 8 wt% surfactant mixture at a Span 80:Tween 80 ratio of 55:45 by volume.

Figure 2b shows an increase in average droplet diameter as the amount of water added increases, which is consistent with our hypothesis. The droplet size increase could potentially imply that the droplets start as surfactant aggregates and swell upon the addition of water. We address this potential mechanism further by analyzing the nanoemulsion microstructure with SANS in the following section.

We then wanted to understand the effect of stir rate on the resulting droplet size. If nanoemulsification occurs due to the swelling of surfactant aggregates such as micelles and vesicles, then the stir rate should have a negligible effect on droplet size.

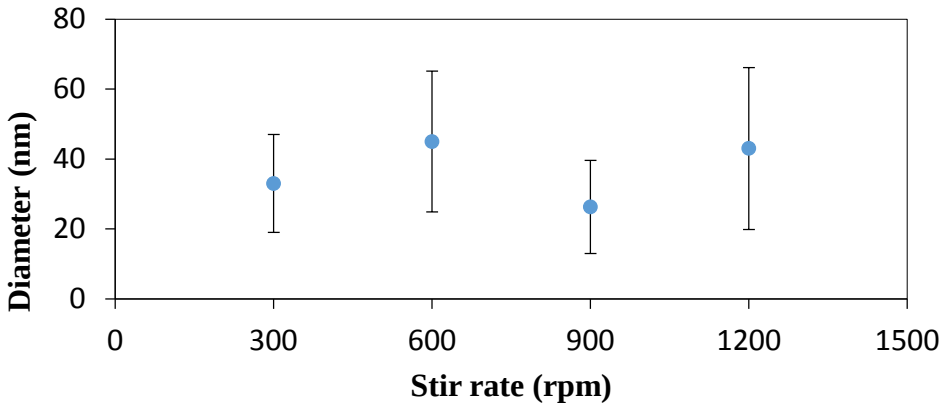

Figure 3. Droplet size with varying stir rate. 10 wt% water is used and 8 wt% surfactant. The Span 80:Tween 80 ratio is 55:45 by volume.

Figure 3 demonstrates how the droplet size changes depending on the stir rate. It is important to note that at 0 rpm, the droplet size was 1200 ± 1000 nm, which is large and highly polydisperse. Upon some stirring, however, it is apparent that droplet sizes are nanoscopic and roughly stir rate-independent, which suggests that mixing primarily keeps the continuous phase well-mixed and prevent recently formed droplets from coalescing.

We then sought to understand the role of stirring time on the resulting droplet size.

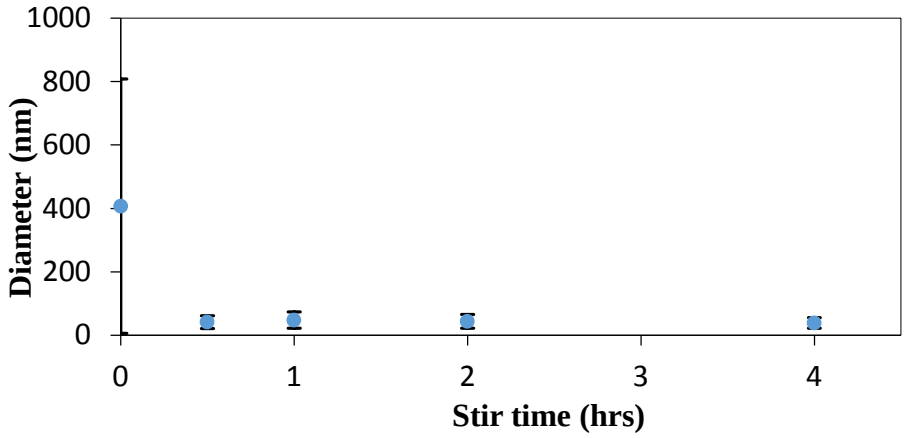

Figure 4. Droplet size with varying stir time. 10 wt% water is used and 8 wt% surfactant. The Span 80:Tween 80 ratio is 55:45 by volume.

Figure 4 demonstrates how the droplet size varies with stir time. The emulsion starts off with an average diameter of 407 ± 401 nm, which is highly polydisperse. The droplet size, however, quickly reduces to 40 nm and the diameter stays at that level for the duration of the experiment. Therefore, the length and intensity of stirring do not matter as much as the act of stirring, which suggests that only keeping the fluid well-mixed, is important for nanoemulsion formation by this method.

While studying the effect of various variables on the initial droplet size gives a better understanding about the nanoemulsion formation mechanism, it cannot provide much information about the stability of the droplets. To study stability, we studied several samples with varying surfactant concentration and examined how the droplet size distributions change over time.

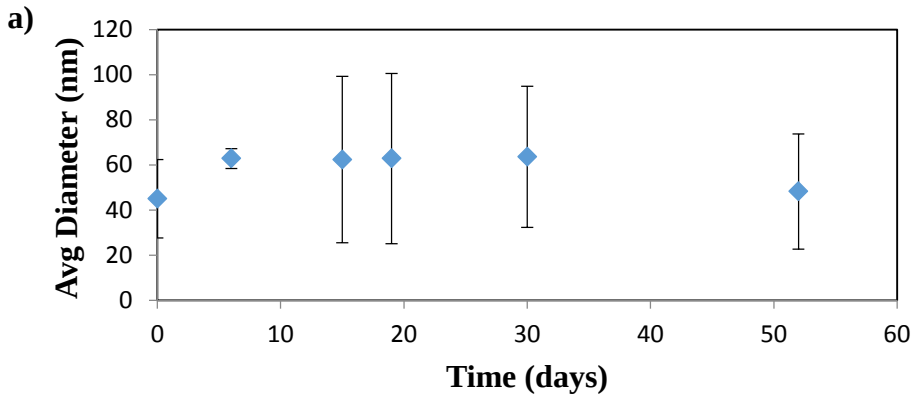

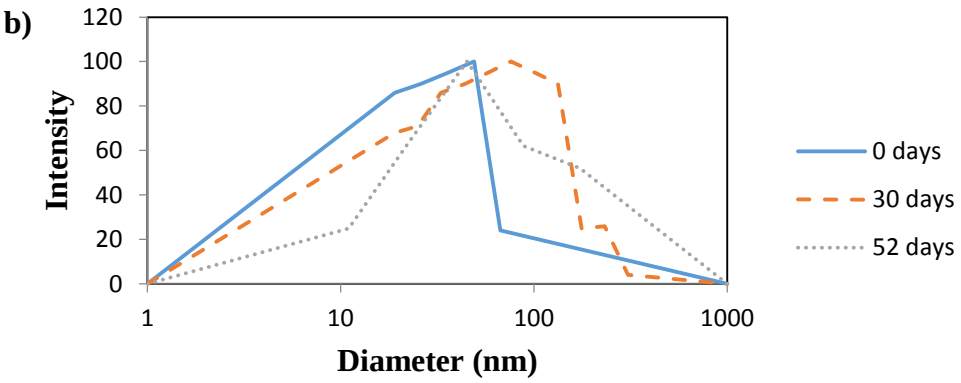

Figure 5. **a)** 4wt% Surfactant, 10 wt% water droplet size over time (does not significantly grow). **b)** Diameter size distributions for 4 wt% surfactant at various times determined using CONTIN analysis.

As seen in Figure 5a, the average diameter of the droplets remains fairly constant over the course of a month. Figure 5b attempts to address the sizes of the most prevalent populations that make up the overall diameter measurements from Figure 5a. A CONTIN analysis is employed in Figure 5b to analyze the different populations within the nanoemulsion, which does Laplace transforms on the scattering data to predict individual modes, or droplet sizes, within a sample. The results in Figure 5b are thus not precise, but can provide some insight into population distributions. From Figure 5b, it appears that overall the population size slowly increases over time and a larger population seems to exist over time. This larger population could result from smaller droplets slowly combining to larger ones. Such slow growth is orders of magnitude lower than the predicted rate of droplet growth via Ostwald Ripening, which has been calculated to be about 100 nm/day. Rate of diameter growth via Ostwald ripening was calculated using the following relation:

$$\frac{dV}{dt} = \frac{8C_\infty \gamma V_m D}{9\rho RT} \quad (1)$$

Where dV/dt is the growth rate of the average droplet volume, C_∞ is the solubility of water in mineral oil, γ is the surface tension, V_m is the molar volume of water, D is the droplet diffusivity, ρ is the density of mineral oil, R is the gas constant, and T is the temperature of the system.

We then studied how the droplet size changed over time at an intermediate surfactant concentration (8 wt%).

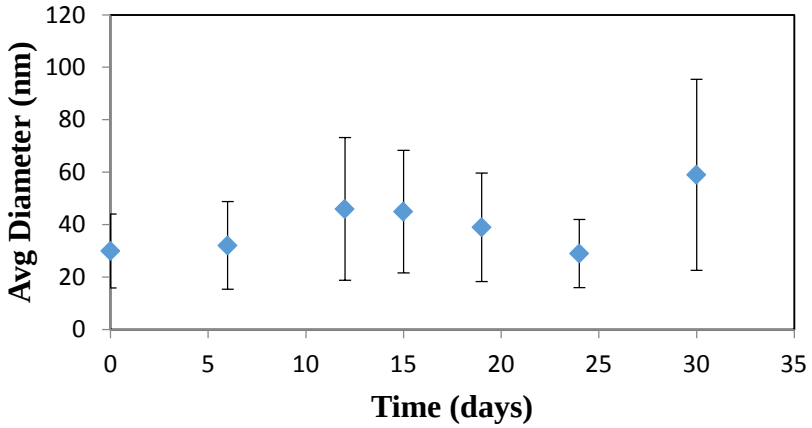

Figure 6. 8 wt% of surfactant, 10 wt% water droplet size over time.

Figure 6 shows the average droplet diameter change over time for 8 wt% surfactant. There is slight growth over a month, which is consistent with the results from 4 wt% surfactant. A calculated rate of Ostwald ripening suggests that the droplets should be growing in size at a rate of 120 nm/day, however it is apparent from the figure that this is not the case. A key assumption of the Ostwald ripening rate equation is that the materials that are growing are spherical droplets. This discrepancy could potentially suggest that the final nanoemulsion is not just made up of droplets, in which the above assumption would be incorrect.

Finally, we looked at how the droplet size changes over time at a high surfactant concentration (15 wt%).

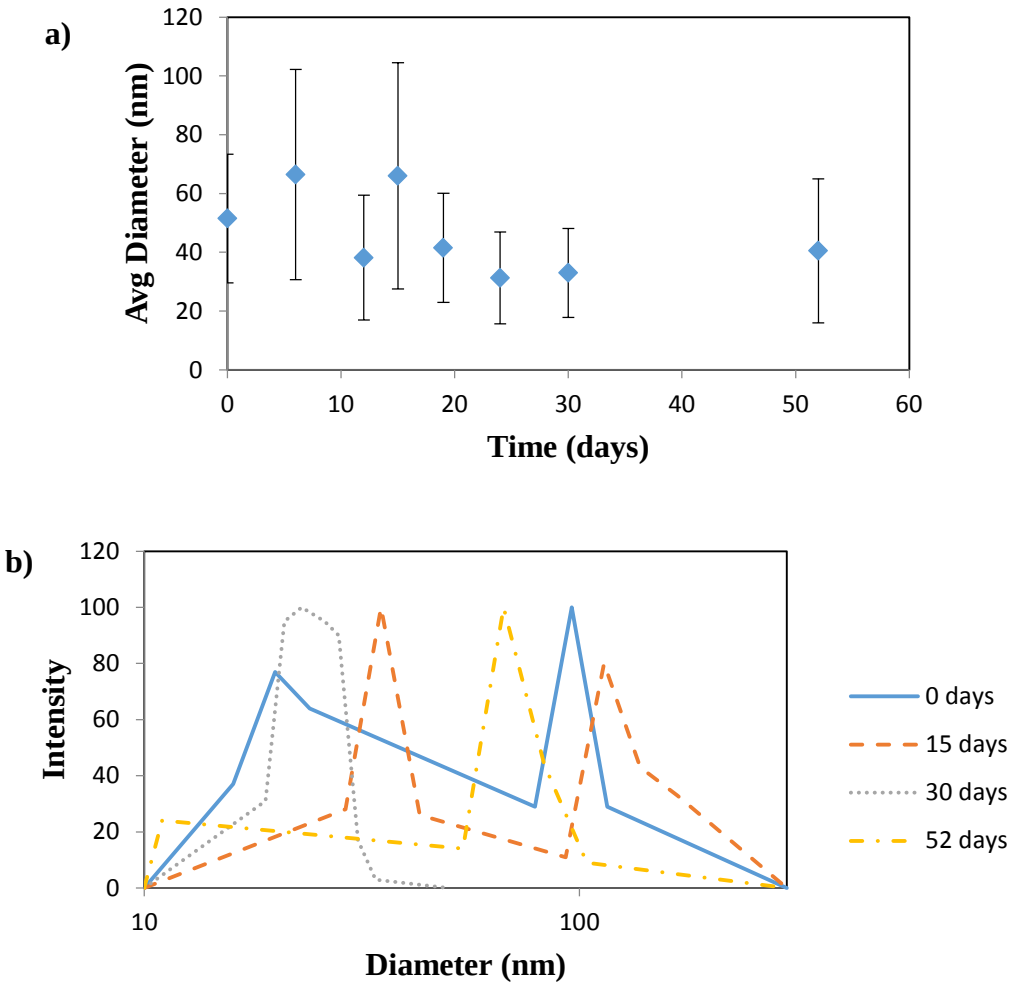

Figure 7. a) 15 wt% surfactant, 10 wt% water droplet size over time. **b)** Diameter size distributions for 15 wt% surfactant at various times determined using CONTIN analysis.

Figure 7a shows the change of average droplet size over time of the 15 wt% surfactant system. The average droplet size stays constant and seems to slightly decrease, which is atypical of droplets growing under Ostwald ripening or coalescence. It is possible that the decrease in reported average droplet size is a result of much larger droplets settling and not being measured by the experiment. Figure 7b shows the typical size distributions of the nanoemulsion droplets at various times as determined using a CONTIN analysis. At t = 0 and 15 days there exists a bimodal distribution of diameters in the emulsion system, which seems to grow over time, with the larger population disappearing after 30 days. This suggests that the larger droplets either

grew too large to be detected using DLS or they represent intermediate phases that later transition to smaller droplets. The latter would require that the nanoemulsification process continues to occur long after stirring has ended. However, since we have little evidence to support this latter hypothesis, we choose to assume the former. Between 30 and 52 days, the monomodal population of droplets increases in size, which is consistent with growth due to Ostwald ripening. However, given the predicted rate of Ostwald ripening ($1.7 * 10^6$ nm^3/day according to Equation 1), and Figure 7a, it is apparent that the average droplet size growth is inconsistent with the rate of Ostwald ripening. This result further suggests that the nanoemulsion may not exist as uniform droplets, but rather a more complex microstructure.

2. Insight into the Nanoemulsion Formation Mechanism

To be able to understand the resulting W/O nanoemulsion properties reported above, it is vital to understand the mechanism by which these emulsions are formed, including the structures of the droplets obtained. If the nanoemulsification process is driven by a thermodynamic pathway, then altering the chemistry of either phase should affect the final state. On the other hand, if the nanoemulsification process is driven by a kinetic pathway, then the chemistry of either phase could potentially be modified without significantly altering the properties of the final state, such as size and stability. We expect that the nanoemulsion is formed using a kinetically driven process and thus depends on the path that the system takes during nanoemulsification.

To understand whether the nanoemulsification process is driven primarily by thermodynamics or kinetics, droplet sizes were measured for nanoemulsions formed under various surfactant:water ratios (SWR). If the emulsification process is driven by equilibrium

thermodynamics, then each SWR would correspond to a single droplet diameter, indicating a single state for each ratio. To graphically determine whether or not a single SWR corresponds with a single droplet diameter, we varied water and surfactant concentrations and superimposed plots of these data looking at how diameter correlates with the SWR.

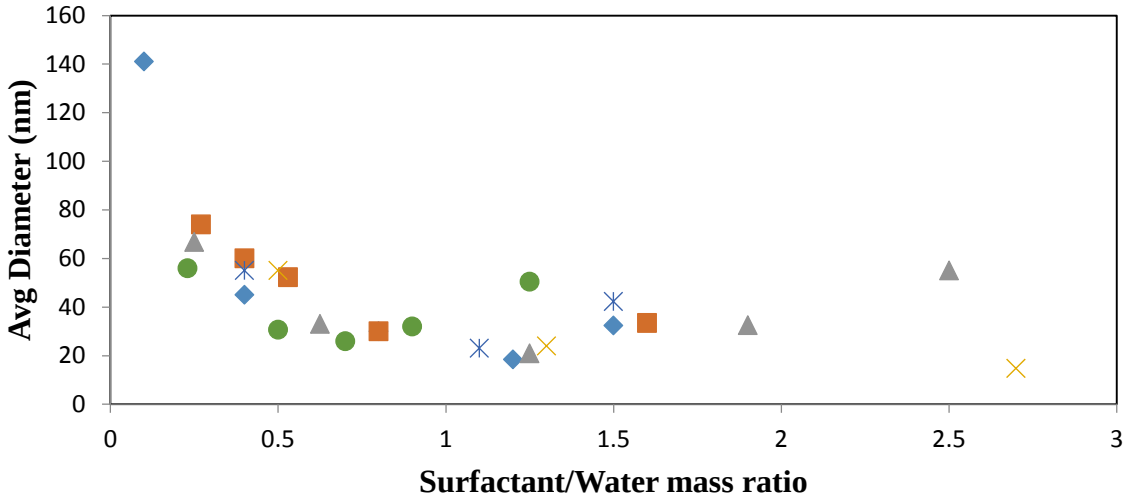

Figure 8. Superposition of droplet size vs SWR shows little correlation between SWR and droplet size.

Figure 8 shows that each SWR does not correspond to a single droplet diameter as evident from the spreading of the data points for each SWR. This implies that the emulsification is probably not driven by equilibrium thermodynamics because the pathway that the system takes to reach the final droplet size distribution determines the final droplet sizes. However, this method does not provide much insight into the specific states or structures that the nanoemulsion evolves during emulsification. Specifically, understanding what surfactant structures are prevalent, whether they are swollen micelles or vesicles with water in the surfactant bilayers, upon addition of water would be vital in understanding the final nanoemulsion state. To begin to understand this, we utilized neutron scattering techniques, specifically SANS.

To understand the structures that develop between an oil/surfactant mixture and a final water-in-oil nanoemulsion, we studied several intermediate steps at two different surfactant concentrations (4 wt% and 15 wt%) using SANS. We initially examined 4 wt% surfactant and 1 wt% D_2O, which represents an early point in the emulsification mechanism.

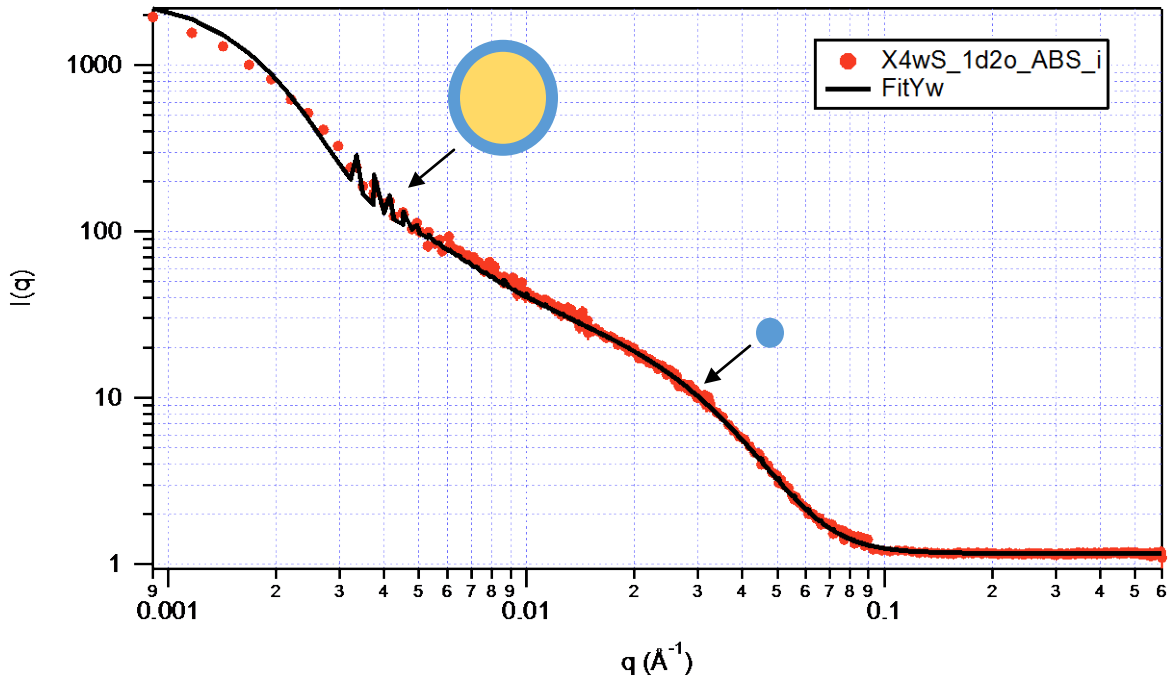

Figure 9a. SANS data for 4 wt% surfactant ~1 wt% D_2O fit to a linear combination of Poly Core-shell and Shultz Spheres models with images depicting the predicted water structures.

Table 1a. Fit parameters for the models used to fit the SANS data in Figure 9a

Volume Fraction (scale)	0.005
mean radius (A)	40
polydisp (sig/avg)	0.450
SLD sphere (A-2)	5.94e-06
SLD solvent (A-2)	-4.32e-07
bkg (cm-1 sr-1)	-1.355
scale	0.014
avg core rad (A)	660
core polydisp (0,1)	0.355
shell thickness (A)	55
SLD core (A-2)	-4.32e-07
SLD shell (A-2)	4.43e-06
SLD solvent (A-2)	-4.32e-07
bkg (cm-1)	2.509

Figure 9a and Table 1a show the SANS spectrum and model parameters for 4 wt % surfactant and only 1 wt% D_2O, which is well below the 10 wt% used to make the final nanoemulsion. As a result this represents an early stage in the nanoemulsification process. The model fit (solid line) is made up of a linear combination of larger, polydisperse core-shell objects [40] and polydisperse Shultz spheres [41, 42] with uniform scattering length density. We hypothesize that the larger objects correspond to vesicles and the smaller objects correspond to droplets, which co-exist in the emulsion. To demonstrate that the combination of models fits the data the best of all reasonable models, we examined simpler models to reduce the number of fit parameters while attempting to preserve fit accuracy. Of the models available, we chose to only study bimodal Shultz spheres and poly core-shell models because they are physically reasonable models for the system.

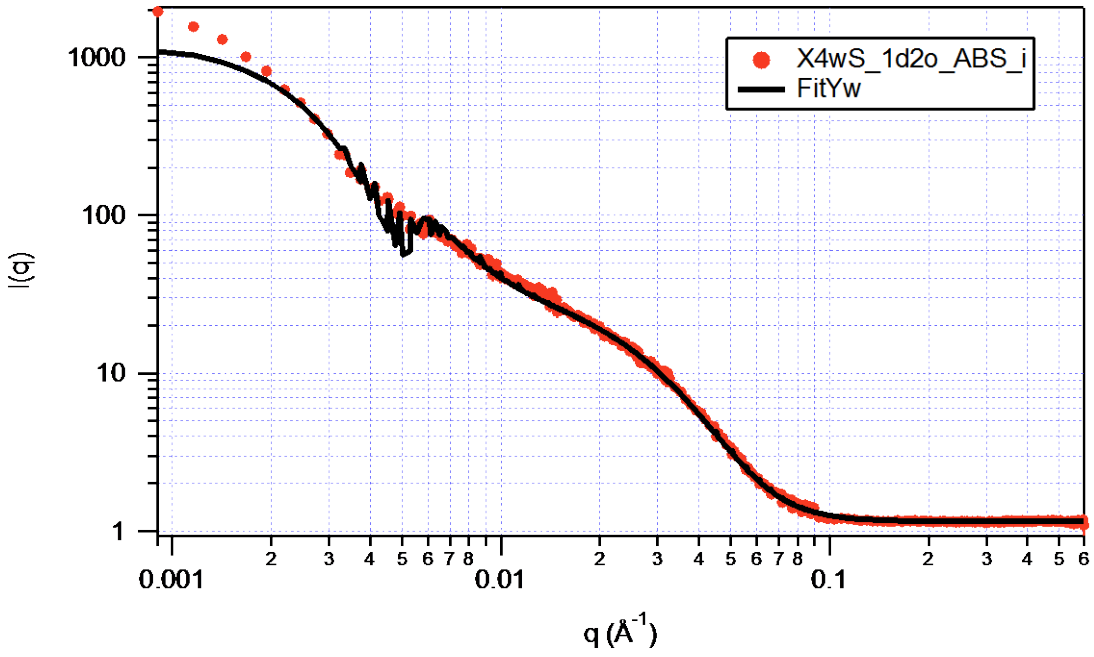

Figure 9b. SANS data for 4 wt% surfactant ~1 wt% D_2O fit to a bimodal Shultz Spheres model.

Table 1b. Fit parameters for the models used to fit the SANS data in Figure 9b

Volume fraction(1)	0.008
Radius (1) (A)	20
polydispersity(1)	-2.76
SLD(1) (A^-2)	1.02e-06
volume fraction(2)	0.076
Radius (2)	30
polydispersity(2)	0.53
SLD(2)	1.35e-06
SLD (solvent)	-4.32e-07
background (cm-1 sr-1)	1.152

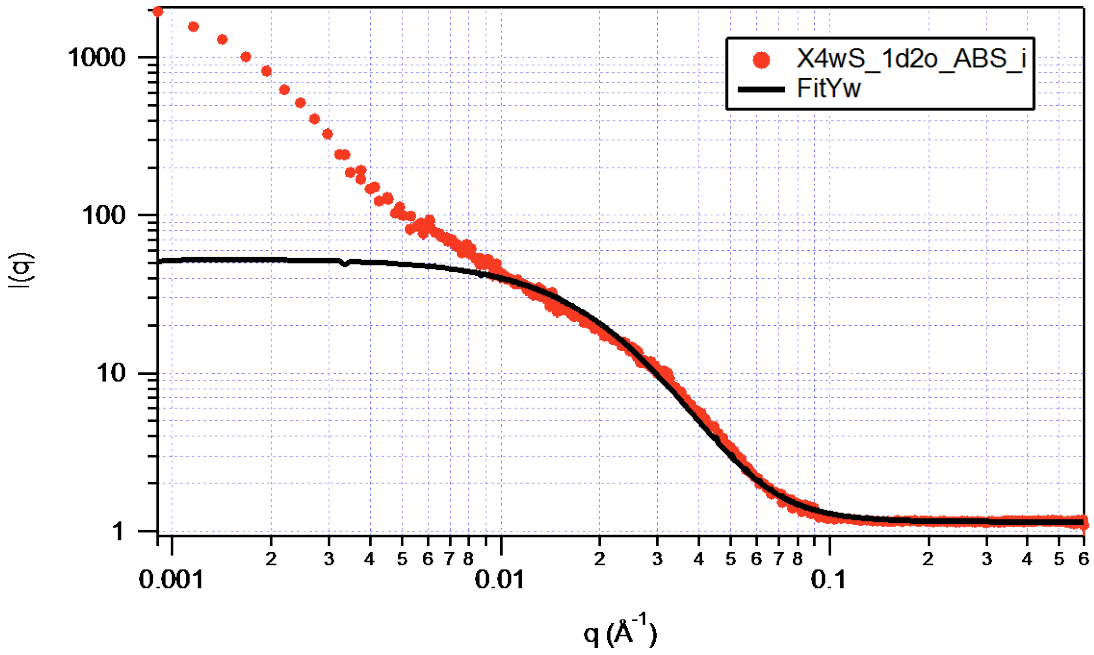

Figure 9c. SANS data for 4 wt% surfactant ~1 wt% D_2O fit to a Poly Core-shell model.

Figure 9b represents the SANS fit for the same sample, but replacing the core-shell model with a second Shultz sphere model to fit the larger objects. It is clearly apparent that the model does not provide as good of a fit the data at q < 0.002 A^{-1}. Figure 9c, on the other hand, represents the SANS fit for the same sample using only a polydisperse core-shell model. This model clearly fails to fit the data for q < 0.03 A^{-}

[1]. Therefore, the best fit comes from a linear superposition of polydisperse core-shell and uniform polydisperse Shultz spheres, which suggests that there is a combination of droplets and vesicles.

The formation of vesicles in low-energy nanoemulsification has been recently imaged in oil-in-water nanoemulsion formation [43], so it is possible that vesicles also exist in this case. From the fit parameters for Figure 9a, we predict that there are droplets of 7 nm in diameter and vesicles that are 130 nm in diameter with a shell thickness of 6 nm. The SLD of the shell ($4.4 * 10^{-6}$) is close to the SLD of D_2O ($3 * 10^{-6}$), which implies that water and surfactants make up the shell. These values are plausible, but unfortunately we cannot confirm the existence of vesicles without direct imaging of the structure (e.g. by cryo-TEM).

We then examined a slightly higher water concentration for 4 wt% surfactant. Specifically, we chose a concentration of water at which the nanoemulsion transitioned from clear to slightly cloudy. We predict that this represents the transition to a higher concentration nanoemulsion and/or a nanoemulsion with larger droplets.

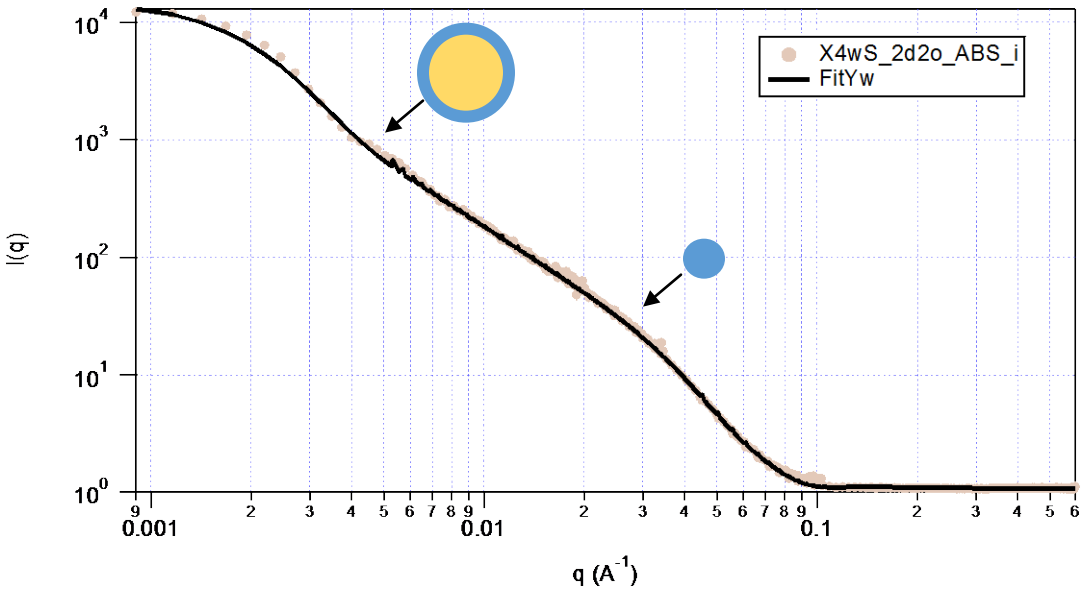

Figure 10. SANS data for 4 wt% surfactant and ~2 wt% D_2O fit to a linear combination of Poly Core Shell and Shultz spheres models with images depicting the predicted water structures.

Table 2. Fit parameters for the model that fits the SANS data in Figure 10.

Volume Fraction (scale)	0.006
mean radius (A)	80
polydisp (sig/avg)	0.087
SLD sphere (A-2)	3.5-06
SLD solvent (A-2)	-4.32e-07
bkg (cm-1 sr-1)	26.82
scale	0.08
avg core rad (A)	440
core polydisp (0,1)	0.481
shell thickness (A)	60
SLD core (A-2)	-4.32e-07
SLD shell (A-2)	4.85e-06
SLD solvent (A-2)	-4.32e-07
bkg (cm-1)	-25.73

Figure 10 represents the data for 4 wt% surfactant and 2wt % D_2O, the point of opacity transition. The data are fit with a linear combination of a polydisperse core-shell and polydisperse Shultz sphere model, as was done in Figure 9a. From the fit parameters, this system seems to be made up of droplets with diameters of about 15 nm and vesicles that have a core diameter of 88 nm and a shell thickness of 6 nm. Given that the diameter of the droplets almost doubles while the shell thickness stays the same, it can be concluded that the excess water swells the droplets.

We then examined the structures of the nanoemulsion at a high surfactant concentration (15 wt%) to identify whether a similar formation mechanism as the low surfactant concentration case would occur. First, we examined a low water concentration (1 wt%) at this high surfactant concentration.

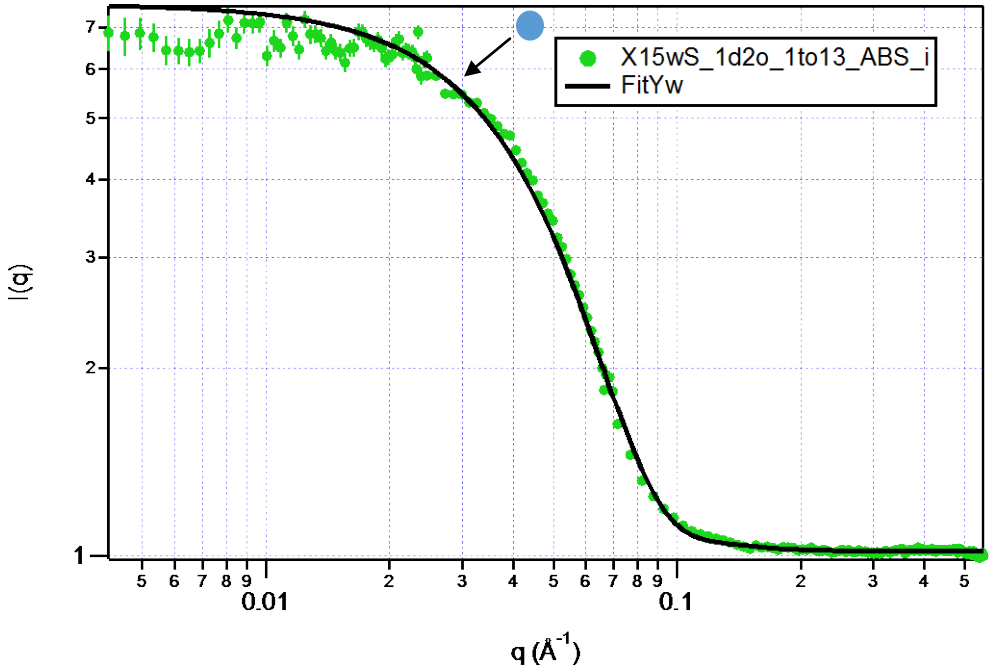

Figure 11. SANS data for 15 wt% surfactant and ~1 wt% D_2O fit to a Shultz sphere model with a depiction of the predicted water structure.

Table 3. Fit parameters for the model fit to the SANS data in Figure 11.

Volume Fraction (scale)	0.028
mean radius (A)	40
polydisp (sig/avg)	0.200
SLD sphere (A-2)	2.25e-06
SLD solvent (A-2)	-4.32e-07
bkg (cm-1 sr-1)	1.018

Figure 11 represents the SANS fit for 15 wt% surfactant and 1 wt% D_2O fit using only a Shultz sphere model. The goodness of the fit without a core-shell model demonstrates that vesicles are not in high enough population at this point to be detected. This suggests that below some critical water/surfactant ratio (between 1/4 and 1/15), only nanoemulsion droplets of approximately 8 nm in diameter exist.

To see if vesicles emerge at a higher water concentration, we added D_2O to the 15 wt% surfactant sample until the clear to slightly turbid transition occurred, which is attributed to an

increase of droplet size and concentration. This transition occurred at a concentration of approximately 4 wt% D_2O.

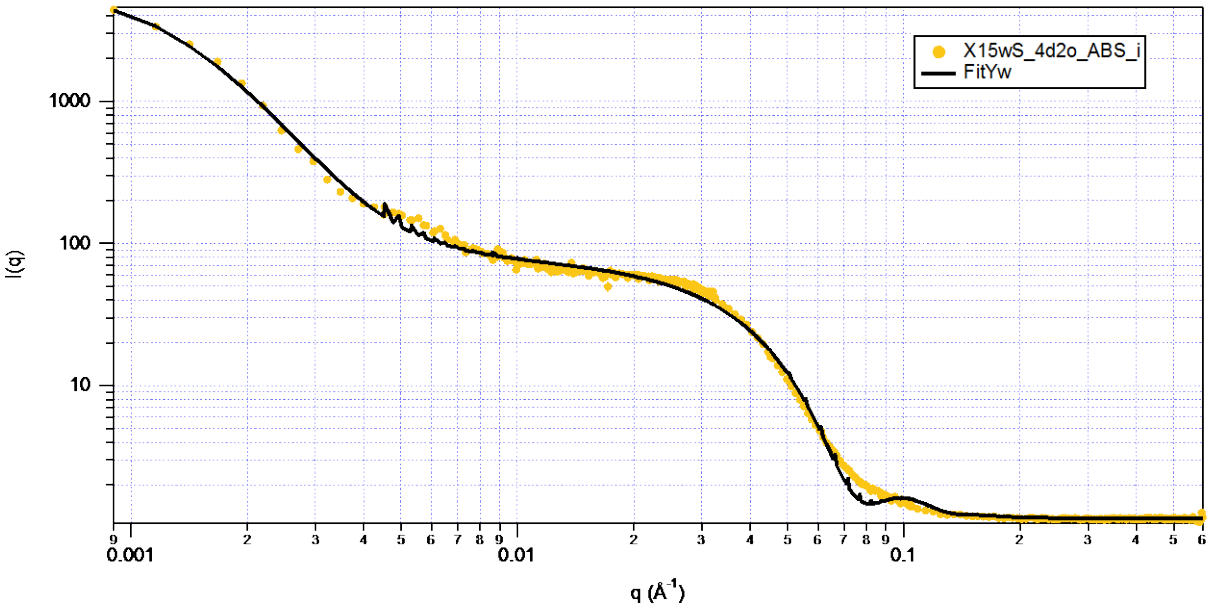

Figure 12a. SANS data for 15 wt% surfactant and ~4 wt% D_2O fit to a linear combination of Poly Core Shell and Shultz Sphere models.

Table 4a. Fit parameters for the model fit to the SANS data in Figure 12a.

Volume Fraction (scale)	0.12
mean radius (A)	60
polydisp (sig/avg)	0.009
SLD sphere (A-2)	2.31e-06
SLD solvent (A-2)	-4.32e-07
bkg (cm-1 sr-1)	1.141
scale	0.71
avg core rad (A)	410
core polydisp (0,1)	0.773
shell thickness (A)	10
SLD core (A-2)	-3.75e-07
SLD shell (A-2)	2.34e-06
SLD solvent (A-2)	-4.32e-07
bkg (cm-1)	0.016

Figure 12a represents the SANS data for 15 wt% surfactant and 4 wt% D_2O fit with a linear combination of polydisperse core-shell and polydisperse Shultz sphere models, as was done in the 4 wt% surfactant cases. However, in this case, the fit does not do well to account for all the

features in the data, specifically the shoulder at q = 0.005 A^{-1} and the oscillation at higher q indicates that the fit could be better and the values derived from the fit could be inaccurate. The shoulder at 0.005 A^{-1} suggests that this model is inadequate. To obtain a better fit, the model was modified to account for this shoulder and to get accurate results for the size of the vesicles.

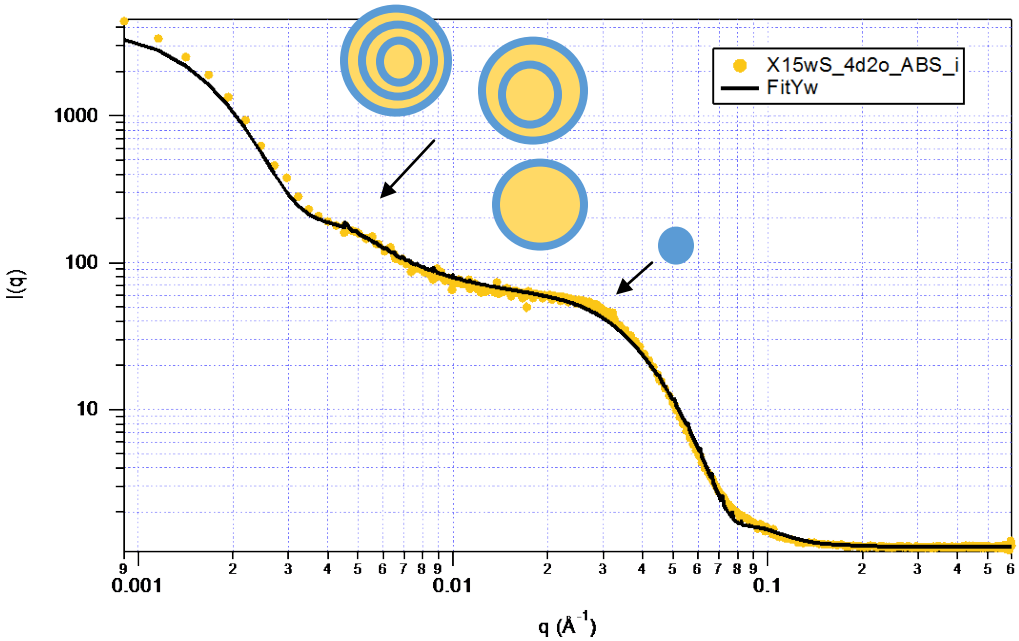

Figure 12b. SANS data for 15 wt% surfactant and ~4 wt% D_2O fit to a linear combination of a Core-3 Shell model and a Shultz Sphere model with images depicting the predicted water structures.

Table 4b. Fit parameters for the model fit to the SANS data in Figure 12b.

Volume Fraction (scale)	0.033
mean radius (A)	50
polydisp (sig/avg)	0.16
SLD sphere (A-2)	4.87e-06
SLD solvent (A-2)	-4.32e-07
bkg (cm-1 sr-1)	0.687
Scale	0.013
avg core rad (A)	690
core polydisp (0,1)	0.313
SLD core (A-2)	-4.32e-07
Shell 1 thickness (A)	40
Shell 1 SLD (A-2)	4.73e-06
Shell 2 thickness (A)	160
Shell 2 SLD (A-2)	-4.32e-07
Shell 3 thickness (A)	50
Shell 3 SLD (A-2)	3.44e-06
SLD solvent (A-2)	-4.32e-07

bkg (cm-1)	0.472

Figure 12b represents the SANS data for the 15 wt% surfactant and 4 wt% D_2O system that is fit to a modified model in which the larger objects are polydisperse, multi-shell objects, and provides a better fit to the data. Thus, we hypothesize from Figure 12b that the nanoemulsion formed under these conditions contains multi-lamellar vesicles with at least two water-swollen bilayers with oil in the core. Comparing Figure 12a and 12b, it seems that adding an extra two shells (need an extra oil shell to separate the two water shalls) to the core-shell model does improve the fit to the data, but this is understandable given the extra parameters. According to the values derived from the fit, the smaller spheres are about 10 nm in diameter and the vesicles have a core diameter of 140 nm, with two effective water shells with a thickness of 4 & 5 nm, and an oil shell between the water shells with a thickness of 16 nm. Whether or not the vesicle is multi- or unilamellar cannot be confirmed without the use of additional probing techniques, such as cryo-TEM. Unfortunately, performing cryo-TEM on oil-based systems is incredibly difficult and requires a level of expertise in TEM that could not be learned in the given time-frame of this work. In the future, it is suggested that cryo-TEM images should be taken of these intermediate structures to confirm whether or not they are indeed vesicles.

Comparing the fit parameters from Table 3 and Table 4b it is apparent that vesicles only appear at sufficiently high water concentration. Moreover, the droplets grow from an average diameter of 8 nm to an average diameter of 10 nm, suggesting that the droplets are being swelled with water. Comparing the volume scales of droplets and vesicles in Table 4b shows that droplets compose about three times the volume of the vesicles. This suggests that the droplets could be more abundant at this point, however, a more systematic SANS experiment would have to be done to fully understand how the concentration of vesicles and droplets change and how their sizes change with respect to water concentration. Such an experiment would have to be done by incrementally increasing the amount of water in the nanoemulsion from 0 wt% to 10 wt% (a typical final concentration of water for our studied nanoemulsions).

E. ***Conclusions & Future Work***

We have developed a stable nanoemulsion system with controlled average particle diameters ranging from 20 to 150 nm that is produced from a low-energy kinetic pathway and seems to form from a mixture of swollen micelles and either unilamellar or multilamellar vesicles. We hypothesize that the kinetic evolution of structure during emulsification is as follows. Upon initial addition of water (the dispersed phase), the water swells the surfactant micelles to produce equilibrium microemulsion droplets. After some critical concentration of water, phase instability occurs, and the surfactant mesophase restructures to form kinetically-stable vesicles with water in the surfactant bilayer. Initially, these vesicles appear to be unilamellar. At higher surfactant concentrations, multilamellar vesicles appear to form. The fact that vesicles are forming suggest that the physicochemical nature of the aqueous phase could affect the formation of the final nanoemulsion. For instance, very high or low pHs, which are needed in some sol-gel syntheses, could cause the nonionic surfactants to gain some ionic character through excess protonation or deprotonation. This change in the surfactant head group chemistry could impact the vesicle properties and alter the final droplet sizes and stability. This property of the nanoemulsion system would limit the synthesis chemistries that could be employed in the droplets. However, if the synthesis reaction occurs faster than the rate of nanoemulsion instability (i.e. droplet or vesicle growth) then the long term stability of the nanoemulsion is irrelevant.

In the future, work must be done to further understand the microstructure of the nanoemulsion system. Specifically, more detailed neutron scattering measurements should be done on the system at a range of water concentrations to better understand the emulsification mechanism. Specifically, we do not currently understand whether or not the final emulsion microstructure is primarily droplets or vesicles. Moreover, understanding how the nanoemulsion microstructure changes over time using SANS will allow us to predict how chemical additives will affect the nanoemulsion stability. Cryogenic-transmission electron microscopy (cryo-TEM) is needed to image these nanoemulsions to verify the microstructure that

is determined by SANS. Specifically, cryo-TEM could confirm the existence of uni- and multi-lamellar vesicles, which are predicted in our SANS analysis.

III. Development of Porous Hydrogels from O/W Nanoemulsion

A. Introduction

Porous materials are in high demand due to their ability to have materials flown through them and their high specific surface areas. These porous materials have already seen applications in drug delivery [44], energy storage [45], catalysis [46], and separations [47]. While porous materials have been made in the past with a variety of techniques, such as micelle-assisted templates [48] or highly packed solid colloid templates[45], using separate liquid phases to template has only recently been considered.

Assembly of liquid droplets could potentially provide a platform for templating porous materials for a variety of applications. A common approach using droplets is to use highly dense, polydisperse macroemulsions as a template for porous foams [13, 49-51]. More recently, work has also been done developing bicontinuous systems using immiscible liquids and particles that jam at the interface of these two liquids [52, 53]. Many of these techniques rely on the arrested phase separation of the liquid phases after applying a temperature above a critical temperature [52, 53]. While work has been done to synthesize materials using these structures [54, 55], these materials have characteristic length scales (pore sizes) between 10-100 μm, but have difficulty approaching sizes smaller than 10 μm. Pore sizes in the 100 nm – 10 μm range are useful for controlling some nanoparticle or large molecule transport, which is a goal of hydrogels for drug delivery applications[44]. The main reasons for the restrictions of past techniques in achieving this length scale is that the technologies either requires solid nanoparticles to jam at the liquid-liquid interface to arrest the phase separation or the system needs large, polydisperse, and

densely packed macroemulsion droplets above the jamming transition to form the template. A potential approach for achieving this size range could be to cause arrested phase separation in nanoscopic droplets, which Professor Helgeson has developed and is continuing to develop [21].

Professor Helgeson has designed a novel technique allowing for thermally reversible gelation of nanoscopic oil droplets [21]. By using hydrophilic polymers with small hydrophobic end groups (e.g. polyethylene glycol diacrylate or PEGDA), it was found that increasing the temperature of an oil-in-water nanoemulsion caused oil drops to exhibit arrested colloidal phase separation[21]. Thus, droplet-rich and droplet-poor domains are formed and the size of these domains is controlled by the temperature used to phase separate the system. If a material were to be grown within the oil or water phase after arrested phase separation, then pore sizes between 100 nm and 10 μm could potentially be reached. The Helgeson lab has done work to understand how the droplet-rich and droplet-poor domains grow over time given an applied temperature above a critical gelation temperature. Previous studies within the Helgeson lab have shown that at increasing temperatures droplets develop attractive interactions but cannot combine into larger droplets due to polymer bridging between droplets [56].

B. Objectives & Approach

Given the prior work done in the Helgeson lab, the goal of my work was to develop a procedure to use the phase separated nanoemulsion in forming porous polymer networks (e.g. hydrogels).

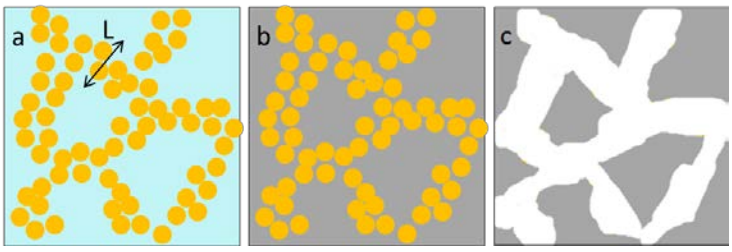

Figure 13. a) Starting with an oil (yellow spheres)-in-water nanoemulsion, arrested phase separation is induced which results in droplet-rich domains (with characteristic length scale L) and droplet-poor domains. b) a polymer is crosslinked within the droplet-poor domains. c) the droplets are evacuated from the system leaving behind a porous hydrogel.

Figure 13 represents the proposed steps to produce porous hydrogel networks using oil-in-water nanoemulsions: the nanoemulsion is first phase separated until the separation is arrested (Figure 13a). After this, the polymer units within the water phase are cross-linked around the droplet-rich domains (Figure 12b). Finally, the droplets are removed from the cross-linked network, leaving behind a porous hydrogel where the large pores are correlated with the size of the droplet-rich domain (Figure 12c). In order to understand how applied temperatures can control macropore sizes in a resulting hydrogel, we must understand how the droplet-rich and poor domains form and what size they grow to. Moreover, we seek to understand how the various processing conditions, such as cross-linking the polymer, affect the domain sizes. Finally, the effectiveness of the porous hydrogels at controlling the diffusivity of molecules and particles must be evaluated to determine whether or not the presence of large pores in hydrogels influences their transport properties.

C. Methods

Oil-in-water nanoemulsions are formed by a well-established procedure in the Helgeson lab [14]. To summarize, a low molecular weight polydimethylsioxane (PDMS) is slowly added to a mixture of water, sodium dodecyl sulfate (SDS) and polyethylene glycol diacrylate (PEGDA) under constant stirring to form a pre-emulsion. The typical composition of materials for this procedure is 33 vol% PEGDA in the aqueous phase, 250 mM SDS, and 33 vol% PDMS droplets. The pre-emulsion is then passed through a high pressure homogenizer many times at homogenization pressures between 10 – 15 kpsi to form the final nanoemulsion.

The droplet size is measured using DLS (as was done with the water-in-oil nanoemulsion) and the rheological properties are studied using a rheometer with a cone and plate geometry. Specifically, a temperature sweep is done while holding the strain rate and the frequency constant to determine the temperature of gelation. Once the gel temperature is known, the kinetics of gelation and the sizes of the arrested droplet-rich and droplet-poor domains can be studied using optical microscopy techniques developed in the Helgeson lab[57]. To produce hydrogels, photocrosslinker is added to a nanoemulsion sample prior to thermal gelation, and the sample is placed in an Al vessel and is kept at a temperature above the gel temperature. After the nanoemulsion phase separation has arrested, UV light is applied to the sample within the vessel for a few seconds to crosslink the PEGDA molecules, thus forming a hydrogel. To study how the crosslinking affects the domain sizes, the sample that is viewed with the optical microscope is also crosslinked using a UV source built into the microscope setup. The domain sizes before and after crosslinking are compared with one another.

To prepare the hydrogel for diffusion studies, the oil within the pores must be extracted. The hydrogels are soaked in ethanol and water to remove excess oil within the pores without de-wetting the hydrogel which could cause uncontrolled pore shrinkage. This rinsing step was done several times to remove as much oil as possible. To prepare the hydrogel samples for diffusion studies using fluorescence recovery after photobleaching (FRAP), the sample is soaked in a hydrophilic dye fluorescein for one day to fully incorporate the dye within the hydrogel network. In the course of performing FRAP studies, a section of the hydrogel is photobleached and the time it takes for the surrounding dye to diffuse into the bleached area is measured, which provides information about the diffusivity within the hydrogel.

D. Results & Discussion

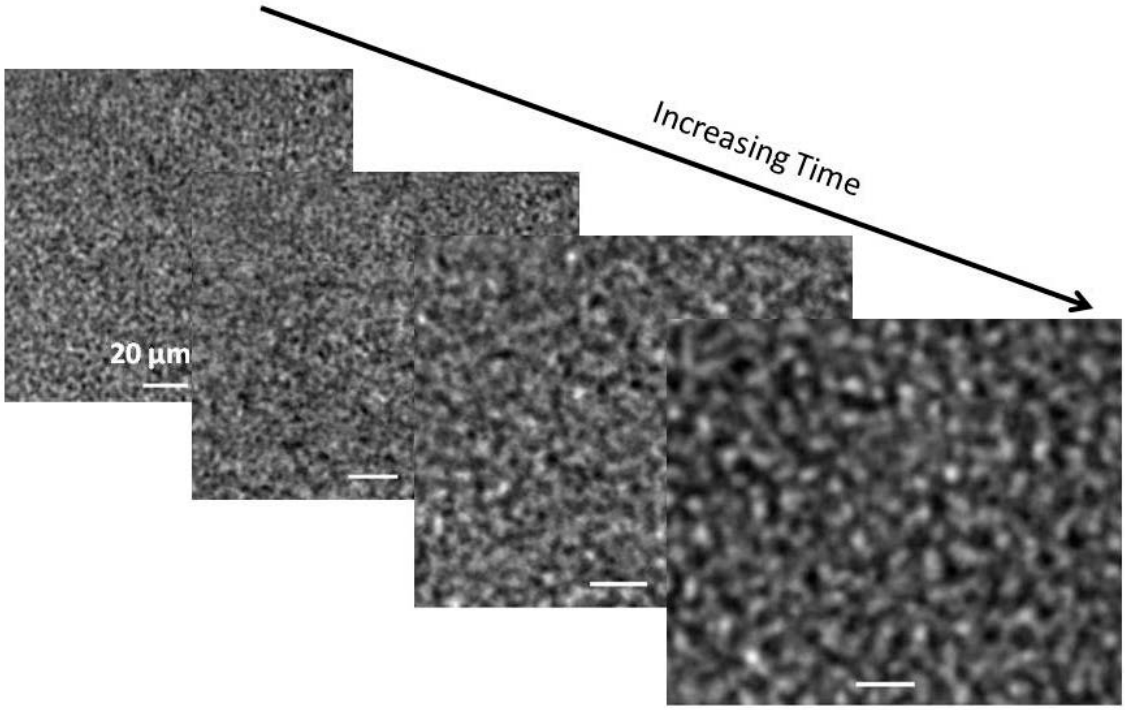

Figure 14. Growth of the light and dark domains over time until the final arrested state is reached. All scale bars are 20 µm and the temperature is $T\text{-}T_{gel}$ = 3 °C.

Figure 14 represents how the nanoemulsions typically change over time while heated. For uninterrupted phase separation, these domains would grow under constant temperature until complete phase separation is achieved. However, in the present case, the interactions between droplets, polymer, and surfactant arrest the phase separation. Thus the domains grow over time until they reach their final size. From Figure 14, it could be deduced that similar domain sizes can be achieved by varying time. However, using the temperature to control domain sizes is

typically more robust since the kinetics of the phase separation are not well understood and can be difficult to control.

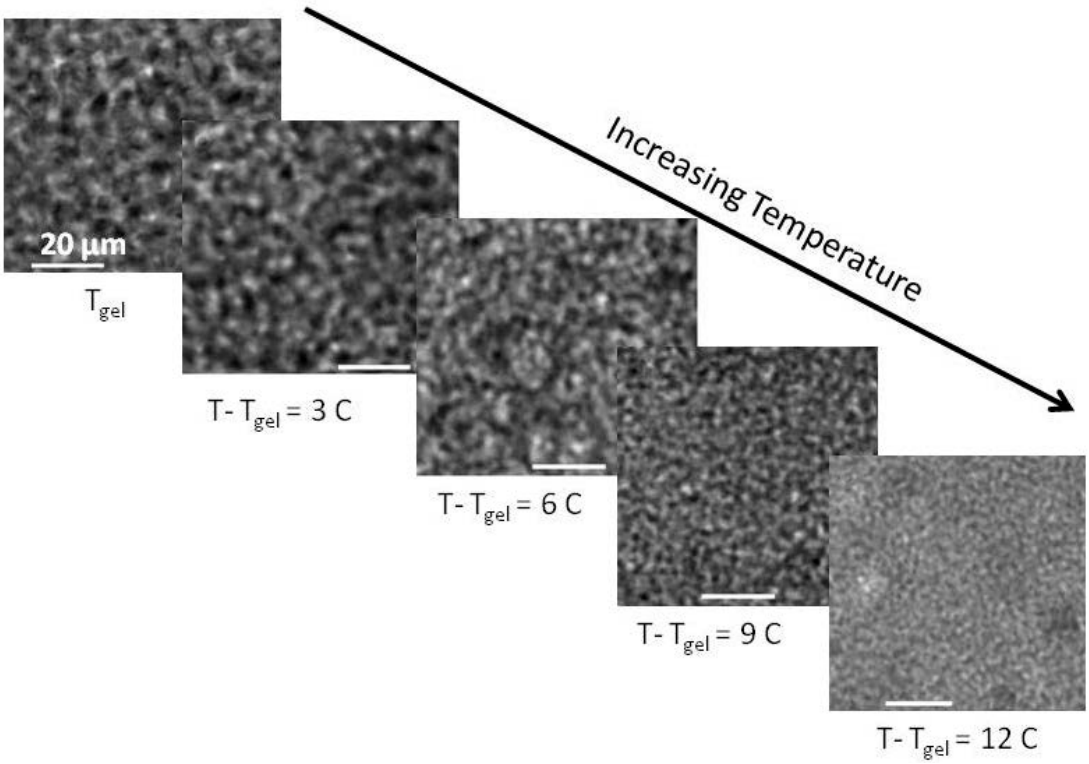

Figure 15. Typical arrested phase separated structure of the nanoemulsion at various temperatures, where T_{gel} is the temperature where this arrested phase separation is first exhibited. All scales bars are 20 µm.

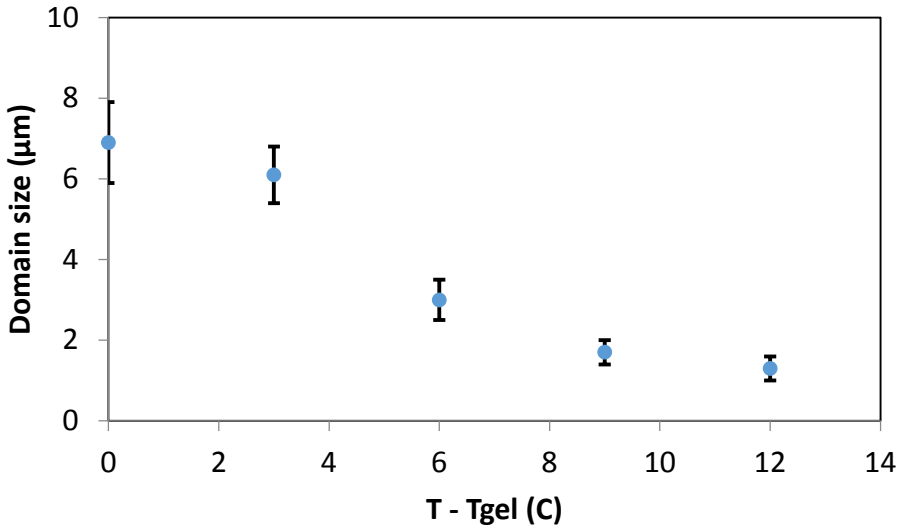

Figure 16. Domain size change for the various temperatures applied to the gelling nanoemulsion. Domain sizes were measured from the images in Figure 14.

Figures 15 & 16 depict how the domain sizes of the nanoemulsion after achieving arrest change with increasing temperature. Domain sizes in Figure 16 were measured using an image processing technique developed in the Helgeson lab. Specifically, it is apparent that both the light and dark domains (representing the droplet rich and droplet-poor domains, respectively) decrease in size as the temperature increases past the gelation temperature (T_{gel}) which is the temperature at which this arrested phase separation is first exhibited. Moreover, from Figure 16, it appears as though the domain sizes start near 7 μm at temperatures close to the gelation temperature, decrease monotonically, but then quickly plateau around 1 μm at higher temperatures. This trend was seen by Helgeson et al [15] and suggests that the final size of the domains could be restricted by the size and number of droplets. Further studies would be needed to indicate what the extent of these relations are.

While knowing how the droplet-rich domain sizes change with temperature and time is important for controlling hydrogel pore sizes, it is vital to also account for how crosslinking of polymer and removal of the oil would affect the sizes. It is anticipated that cross-linking of the polymer within the droplet-poor domains should cause a slight increase in pressure exerted on the droplets, which could cause the droplet rich domains to constrict. Moreover, drying of the hydrogel is known to constrict pore sizes as the polymer network starts to collapse, so ensuring that the hydrogel remains hydrated during oil removal is key to preserving the desired pore sizes.

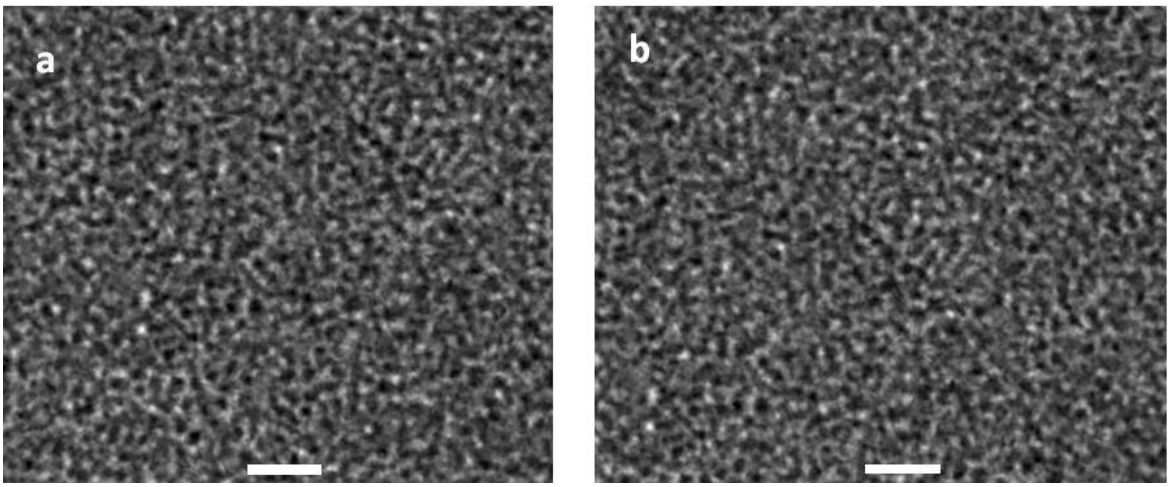

Figure 17. a) nanoemulsion exhibiting arrested phase separation, b) nanoemulsion after cross-linking PEGDA within the droplet-poor domains of the arrested phase separation structure. All scale bars are 20 µm

Figure 17 consists of images before (a) and after (b) crosslinking shows that the droplet-rich domain sizes do not significantly change due to crosslinking.

After removal of the droplets, while maintaining hydration of the hydrogel network, the effectiveness of the porous hydrogel formation procedure is tested using diffusion studies. Specifically, if the hydrogel has much larger pores due to forming around the droplet-rich domain compared to a hydrogel without droplets, then there should be a significant change in the diffusivity of a dye molecule or particle.

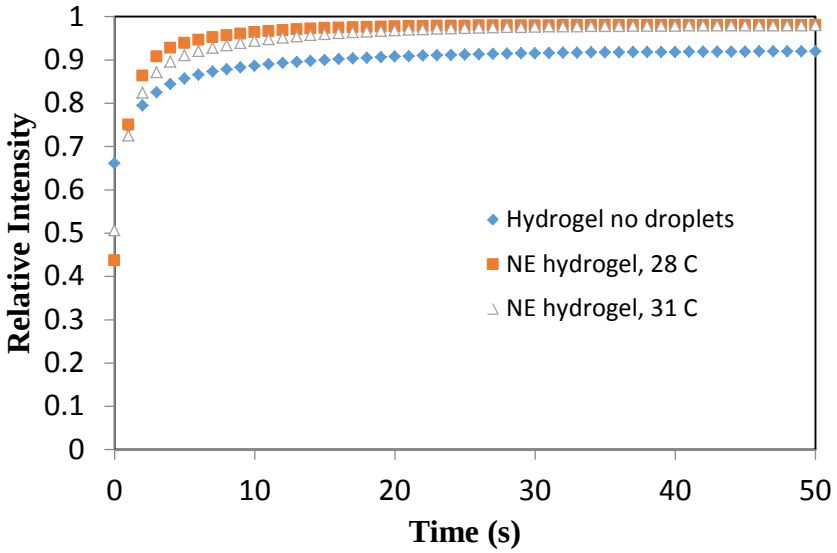

Figure 18. Intensity measurement over time of a photo-bleached region of hydrogel samples as a fluorescent dye diffuses into the region of study.

Table 5. Diffusion times and pre-exponential factors determined by a double exponential model for dyes in the hydrogels

Sample	t_1 (s^{-1})	A_1	t_2 (s^{-1})	A_2
Control (no macropores)	1.69	-0.17	10.2	-0.089
NE hydrogel, 28 C	0.92	-0.45	5.81	-0.096
NE hydrogel, 31 C	1.17	-0.36	8.78	-0.114

Figure 18 represents FRAP data, where a plot of the normalized integrated fluorescence intensity in a circular photo-bleached area is plotted over time in several porous hydrogels. The dye molecule is very small compared to the size of the droplet-rich domains and thus minor differences between the sizes of the pores left by these domains are not detected. The hydrogels formed using this procedure (filled squares and open triangles) allowed for the dye in the photo bleached region to return to its initial concentration. The control, which had only the nanoscopic pores of the hydrogel network (filled diamonds) did not allow for the dye to return to its initial concentration. Thus the control had greater excluded volume in its network than the hydrogels made through the described procedure, implying that the procedure did create porous hydrogels. Table 5 represents diffusion times for the dye molecules in each of the hydrogel networks as determined by fitting the data to a double exponential. From the table it is apparent that the diffusion times decrease as the pore sizes increase (the NE arrested at 28 C has the largest pores), so the diffusivity of dye molecules in the hydrogels with larger macropores is greater than the diffusivity in the hydrogel with small or no macropores. This preliminary data implies that the mass transport of molecules can be controlled by altering the temperature used to arrest the NE. More work must be done, however, to determine how the diffusion of drug nanoparticles would be affected by these pores.

E. Conclusion & Future Work

We have developed a procedure to form porous hydrogel networks that could be used for drug delivery applications. We have a preliminary understanding of how the droplet-rich domains form within a nanoemulsion network and how the steps of the procedure (i.e. cross-linking and droplet extraction) affect the final domain sizes. However, much more work must be done to develop a stronger understanding of the exact ways that these steps affect the pore sizes of the network. More work must also be done to thoroughly understand the mechanism of the arrested phase separation with the hope of developing a predictive model to determine pore sizes based on certain conditions. This would allow for greater control over porosity in hydrogel networks and could allow them to be specifically modified for desired applications. Additionally, environmental scanning electron microscopy (ESEM) should be used to image the final hydrogel network. ESEM has capabilities to image hydrated materials, which is ideal for hydrogel networks as drying the network for SEM would irreversibly constrict the network and collapse pores. As a result, normal SEM images do not represent the true properties of the hydrogel. Finally, more work must be done to identify the capabilities of these hydrogel networks in drug delivery applications. As eluded to before, more FRAP studies should be employed using fluorescently labeled nanoparticles of various sizes to better understand how the porous networks affect the diffusivity of drug particles.

The developed procedure, however, could also be used for applications in separations, catalysis, or even energy technologies. Specifically, work should be done to explore growing networks of materials that undergo sol-gel reactions, such as silica or titania, around the droplet-rich domains. The result should be solid networks with pore sizes that mimic the droplet-rich domain sizes. In addition, these networks would be rigid, so the pores should not shrink significantly during processing. Additionally, materials could even be grown in the droplet-rich

domains by having a precursor material in the droplet. For instance, by having a cross-linkable hydrophobic polymer (e.g. PDMS) within the droplets, a porous hydrophobic polymer network could also be formed.

IV. Conclusions & Future Work

A. Conclusions

This work was aimed at understanding the fundamentals of nanoemulsions (i.e. how they form spontaneously) while also using them to control material growth. My studies have elucidated some possible routes and mechanisms for the spontaneous emulsification of water-in-oil nanoemulsions. The revelation that vesicles could be forming during emulsion formation, rather than just droplets, implies that the physicochemical nature of the water phase does matter for nanoemulsion formation. For instance, if a highly basic water phase was added, then the surfactant heads could deprotonate and repel each other, potentially causing the vesicles and the final nanoemulsion to change in size and stability. From this knowledge, we can gain insight into how a particle precursor in the droplet would affect the droplet and particle sizes.

Apart from working on the fundamental aspects of nanoemulsion formation, my work has also involved using a well-developed nanoemulsion system to design an application. I have explored the use of arrested phase separation in nanoemulsions developed in the Helgeson lab to control the growth of porous hydrogels. Porous hydrogels were formed using the developed technique and these template pores significantly affected the diffusivity of molecules compared to a hydrogel formed in an aqueous environment without oil droplets. Moreover, there was a noticeable difference in the length scales of porosity and transport in templated hydrogels given the temperature used to arrest the nanoemulsion. Specifically, hydrogels with smaller pores had lower diffusivity of a dye molecule than the hydrogels with larger pores. Thus, the developed technique could be effective at producing hydrogels for drug delivery applications by tailoring pore size depending on the drug molecule or particle to be stored or released.

B. Future Work

While my work has elucidated a potential mechanism for low-energy water-in-oil nanoemulsion formation, more work must be done to confirm the results. Specifically, the SANS data on its own does not prove that vesicles are forming during emulsion formation. To confirm this interpretation, another *in situ* technique, such as cryo-TEM must be used to image the emulsions. If vesicles exist, then a core-shell structure with different contrasts should be visible. However, cryo-TEM in a low-boiling, hydrophobic solvent is a persistent challenge. Overcoming this challenge would help elucidate the formation mechanism of the developed water-in-oil nanoemulsion.

Given that these emulsions consist of water droplets, the next step would be to pursue the synthesis of nanoparticles (e.g. of silica) within these droplets. By correlating droplet size with particle size, it can be determined whether the droplets act as sufficient containers for the growth of nanoparticles. If the droplets can control the spherical particle size, then future endeavors could work toward growing anisotropic nanoparticles. This would require the use of external fields or additives to allow for directional growth of the particles.

While my work on the use of nanoemulsions as tools for porous hydrogel development has demonstrated that these pore sizes can be controlled, more work must be done to determine the extent to which they can be controlled. More data would aid in the construction of an empirical model correlating the temperature relative to the gel temperature used to arrest the nanoemulsion phase separation and the dominant length scale of the arrested droplet-rich domain. Additionally, a quantitative correlation must be established between the original size of the droplet-rich domains and the final size of the hydrogel pore sizes. Environmental SEM will be useful to accurately measure the size of the pores in the hydrogel, since the hydrogel won't

need to be dried which would shrink the pores. With all this analysis, the pore sizes of the hydrogels could be predicted based on the processing temperature of the nanoemulsion.

These porous hydrogels have excellent potential applications in drug delivery due to the biologically benign nature of the polymer and the size control of the pore sizes to be between 1 and 10 μm. More work must be done, however, to determine how effectively the pores restrict movement of molecules and particles to emulate how drugs would diffuse out of the pores during encapsulation and delivery. The bicontinuous nature of the arrested phase separation of these nanoemulsions also gives it potential uses in templating porous ceramics, such as silica. By growing materials either in the droplet-poor domains (e.g. silica) or the droplet-rich domains (e.g. a cross-linkable PDMS) then this property of the nanoemulsion has the potential to produce a wide-range of porous materials.

References

1. Qian, C., et al., *Inhibition of beta-carotene degradation in oil-in-water nanoemulsions: Influence of oil-soluble and water-soluble antioxidants.* Food Chemistry, 2012. **135**(3): p. 1036-1043.
2. Ragelle, H., et al., *Nanoemulsion formulation of fisetin improves bioavailability and antitumour activity in mice.* International Journal of Pharmaceutics, 2012. **427**(2): p. 452-459.
3. Wang, L.J., et al., *Design and optimization of a new self-nanoemulsifying drug delivery system.* Journal of Colloid and Interface Science, 2009. **330**(2): p. 443-448.
4. Gulotta, A., et al., *Nanoemulsion-Based Delivery Systems for Polyunsaturated (omega-3) Oils: Formation Using a Spontaneous Emulsification Method.* Journal of Agricultural and Food Chemistry, 2014. **62**(7): p. 1720-1725.
5. Zheng, W.W., et al., *Preparation and the in Vitro Evaluation of Nanoemulsion System for the Transdermal Delivery of Granisetron Hydrochloride.* Chemical & Pharmaceutical Bulletin, 2010. **58**(8): p. 1015-1019.
6. Bilbao-Sainz, C., et al., *Nanoemulsions Prepared by a Low-Energy Emulsification Method Applied to Edible Films.* Journal of Agricultural and Food Chemistry, 2010. **58**(22): p. 11932-11938.
7. El Kinawy, O.S., S. Petersen, and J. Ulrich, *Technological Aspects of Nanoemulsion Formation of Low-Fat Foods Enriched with Vitamin E by High-Pressure Homogenization.* Chemical Engineering & Technology, 2012. **35**(5): p. 937-940.
8. Ghosh, V., A. Mukherjee, and N. Chandrasekaran, *Eugenol-loaded antimicrobial nanoemulsion preserves fruit juice against, microbial spoilage.* Colloids and Surfaces B-Biointerfaces, 2014. **114**: p. 392-397.
9. Wang, L.J., et al., *Oil-in-water nanoemulsions for pesticide formulations.* Journal of Colloid and Interface Science, 2007. **314**(1): p. 230-235.
10. Machado, A.H.E., et al., *Preparation of Calcium Alginate Nanoparticles Using Water-in-Oil (W/O) Nanoemulsions.* Langmuir, 2012. **28**(9): p. 4131-4141.
11. Alvarado, A.G., *Poly(hexyl methacrylate) Nanoparticles Templating in Nanoemulsions-Made by Phase Inversion Temperature.* Journal of Macromolecular Science, Part A: Pure and Applied Chemistry, 2013: p. 7.
12. Butler, M.A., P.F. James, and J.D. Jackson, *An emulsion method for producing fine, low density, high surface area silica powder from alkoxides.* Journal of Materials Science, 1996. **31**(7): p. 1675-1680.
13. Hessien, M., et al., *Nanocrystalline iron oxide synthesised within Hierarchical Porous Silica prepared by nanoemulsion templating.* Chemical Communications, 2012. **48**(80): p. 10022-10024.
14. Hu, W.C., et al., *One-step synthesis of silica hollow particles in a W/O inverse emulsion.* Colloid and Polymer Science, 2013. **291**(11): p. 2697-2704.
15. Landfester, K., *Miniemulsion Polymerization and the Structure of Polymer and Hybrid Nanoparticles.* Angewandte Chemie-International Edition, 2009. **48**(25): p. 4488-4507.
16. Porras, M., et al., *Ceramic particles obtained using W/O nano-emulsions as reaction media.* Colloids and Surfaces a-Physicochemical and Engineering Aspects, 2005. **270**: p. 189-194.
17. Anton, N. and P. Saulnier, *Adhesive water-in-oil nano-emulsions generated by the phase inversion temperature method.* Soft Matter, 2013. **9**(28): p. 6465-6474.
18. Anton, N. and T.F. Vandamme, *The universality of low-energy nano-emulsification.* International Journal of Pharmaceutics, 2009. **377**(1-2): p. 142-147.

19. Izquierdo, P., et al., *The influence of surfactant mixing ratio on nano-emulsion formation by the pit method.* Journal of Colloid and Interface Science, 2005. **285**(1): p. 388-394.
20. Bouchemal, K., et al., *Nano-emulsion formulation using spontaneous emulsification: solvent, oil and surfactant optimisation.* International Journal of Pharmaceutics, 2004. **280**(1-2): p. 241-251.
21. Helgeson, M.E., et al., *Mesoporous organohydrogels from thermogelling photocrosslinkable nanoemulsions.* Nature Materials, 2012. **11**(4): p. 344-352.
22. Nam, Y.S., et al., *Nanosized Emulsions Stabilized by Semisolid Polymer interphase.* Langmuir, 2010. **26**(16): p. 13038-13043.
23. Sugumar, S., et al., *Ultrasonic emulsification of eucalyptus oil nanoemulsion: Antibacterial activity against Staphylococcus aureus and wound healing activity in Wistar rats.* Ultrasonics Sonochemistry, 2014. **21**(3): p. 1044-1049.
24. McClements, D.J., *Nanoemulsions versus microemulsions: terminology, differences, and similarities.* Soft Matter, 2012. **8**(6): p. 1719-1729.
25. Nazarzadeh, E., T. Anthonypillai, and S. Sajjadi, *On the growth mechanisms of nanoemulsions.* Journal of Colloid and Interface Science, 2013. **397**: p. 154-162.
26. Israelachvili, J.N., *Intermolecular and surface forces*. 3rd ed. 2011, Burlington, MA: Academic Press. xxx, 674 p.
27. An, H.Z., M. Helgeson, and P.S. Doyle, *Nanoemulsion Composite Microgels for Orthogonal Encapsulation and Release.* Advanced Materials, 2012. **24**(28): p. 3838.
28. Peng, L.C., et al., *Optimization of water-in-oil nanoemulsions by mixed surfactants.* Colloids and Surfaces a-Physicochemical and Engineering Aspects, 2010. **370**(1-3): p. 136-142.
29. Porras, M., et al., *Studies of formation of W/O nano-emulsions.* Colloids and Surfaces a-Physicochemical and Engineering Aspects, 2004. **249**(1-3): p. 115-118.
30. Porras, M., et al., *Properties of water-in-oil (W/O) nano-emulsions prepared by a low-energy emulsification method.* Colloids and Surfaces a-Physicochemical and Engineering Aspects, 2008. **324**(1-3): p. 181-188.
31. El-Din, M.R.N., *Study on the stability of water-in-kerosene nano-emulsions and their dynamic surface properties.* Colloids and Surfaces a-Physicochemical and Engineering Aspects, 2011. **390**(1-3): p. 189-198.
32. El-Din, M.R.N. and A.M. Al-Sabagh, *Preparation of Water-in-Hexane Nanoemulsions Using Low Energy Emulsification Method.* Journal of Dispersion Science and Technology, 2012. **33**(1-3): p. 68-74.
33. Tadros, T., et al., *Formation and stability of nano-emulsions.* Advances in Colloid and Interface Science, 2004. **108**: p. 303-318.
34. Wu, H.L., et al., *Topical transport of hydrophilic compounds using water-in-oil nanoemulsions.* International Journal of Pharmaceutics, 2001. **220**(1-2): p. 63-75.
35. Shakeel, F. and W. Ramadan, *Transdermal delivery of anticancer drug caffeine from water-in-oil nanoemulsions.* Colloids and Surfaces B-Biointerfaces, 2010. **75**(1): p. 356-362.
36. Hwang, T.L., et al., *Permeation Enhancer-Containing Water-In-Oil Nanoemulsions as Carriers for Intravesical Cisplatin Delivery.* Pharmaceutical Research, 2009. **26**(10): p. 2314-2323.
37. Uson, N., M.J. Garcia, and C. Solans, *Formation of water-in-oil (W/O) nano-emulsions in a water/mixed non-ionic surfactant/oil systems prepared by a low-energy emulsification method.* Colloids and Surfaces a-Physicochemical and Engineering Aspects, 2004. **250**(1-3): p. 415-421.
38. Kline, S.R., *Reduction and analysis of SANS and USANS data using IGOR Pro.* Journal of applied crystallography, 2006. **39**(6): p. 5.

39. Komaiko, J. and D.J. McClements, *Optimization of isothermal low-energy nanoemulsion formation: Hydrocarbon oil, non-ionic surfactant, and water systems.* Journal of Colloid and Interface Science, 2014. **425**: p. 59-66.
40. Bartlett, P. and R.H. Ottewill, Journal of Chemical Physics, 1992. **96**: p. 1.
41. Schulz, G.V., Physical Chemistry, 1935. **43**: p. 1.
42. Kotlarchyk, M. and S.-H. Chen, Journal of Chemical Physics, 1983. **79**: p. 8.
43. Lee, H.S., et al., *Cryogenic Electron Microscopy Study of Nanoemulsion Formation from Microemulsions.* Langmuir, 2014. **30**(36): p. 7.
44. Ma, X., et al., *Drug release behaviors of a pH/thermo-responsive porous hydrogel from poly(N-acryloylglycinate) and sodium alginate.* Journal of Sol-Gel Science and Technology, 2013. **68**(2): p. 356-362.
45. Zhang, H.G., X.D. Yu, and P.V. Braun, *Three-dimensional bicontinuous ultrafast-charge and -discharge bulk battery electrodes.* Nature Nanotechnology, 2011. **6**(5): p. 277-281.
46. Sung, I.K., et al., *Tailored macroporous SiCN and SiC structures for high-temperature fuel reforming.* Advanced Functional Materials, 2005. **15**(8): p. 1336-1342.
47. Tanaka, N., et al., *Monolithic silica columns for high-efficiency chromatographic separations.* Journal of Chromatography A, 2002. **965**(1-2): p. 35-49.
48. Zhao, D.Y., et al., *Triblock copolymer syntheses of mesoporous silica with periodic 50 to 300 angstrom pores.* Science, 1998. **279**(5350): p. 548-552.
49. Esquena, J., G.R. Sankar, and C. Solans, *Highly concentrated W/O emulsions prepared by the PIT method as templates for solid foams.* Langmuir, 2003. **19**(7): p. 2983-2988.
50. Zhang, H.F. and A.I. Cooper, *Synthesis and applications of emulsion-templated porous materials.* Soft Matter, 2005. **1**(2): p. 107-113.
51. Cameron, N.R., *High internal phase emulsion templating as a route to well-defined porous polymers.* Polymer, 2005. **46**(5): p. 1439-1449.
52. Herzig, E.M., et al., *Bicontinuous emulsions stabilized solely by colloidal particles.* Nature Materials, 2007. **6**(12): p. 966-971.
53. Lee, M.N., et al., *Making a Robust Interfacial Scaffold: Bijel Rheology and its Link to Processability.* Advanced Functional Materials, 2013. **23**(4): p. 417-423.
54. Lee, M.N. and A. Mohraz, *Bicontinuous Macroporous Materials from Bijel Templates.* Advanced Materials, 2010. **22**(43): p. 4836-+.
55. Lee, M.N. and A. Mohraz, *Hierarchically Porous Silver Monoliths from Colloidal Bicontinuous Interfacially Jammed Emulsion Gels.* Journal of the American Chemical Society, 2011. **133**(18): p. 6945-6947.
56. Helgeson, M.E., et al., *Homogeneous percolation versus arrested phase separation in attractively-driven nanoemulsion colloidal gels.* Soft Matter, 2014. **10**(17): p. 3122-3133.
57. Gao, Y. and M.E. Helgeson, *Texture analysis microscopy: quantifying structure in low-fidelity images of dense fluids.* Optics Express, 2014. **22**(8): p. 10046-10063.